JP1.12

Aerosol Indirect Effect on Long-lasting Mesoscale Convective Systems: A Modeling Study

Xiaowen Li[1,2], Wei-Kuo Tao[1], Alexander Khain[3], Joanne Simpson[1]

[1]NASA/GSFC; [2]GEST center, University of Maryland, Baltimore County; [3]The Hebrew University of Jerusalem

1. INTRODUCTION

The theory of aerosol indirect effect was proposed by Twomey back in 70s (e.g., Twomey, 1977, Twomey et al., 1984). Twomey hypothesized that increasing the number concentration of cloud condensation nuclei (CCN) can result in increased cloud droplet number and reduced *cloud drop sizes. Assuming the same amount of liquid water content, more and smaller cloud droplets will increase cloud albedo, producing a cooling effect on the surface temperature. Furthermore, rain formation will be suppressed when the cloud drop size is reduced, extending the cloud lifetime. This will further reduce the solar radiation received on the earth surface.

The most convincing evidences of the aerosol indirect effect come from observations of ship tracks and their rain suppression effect (e.g., Coakley et al., 1987, Ferek et al., 2000). The ship track effect happens in stable oceanic environment where the updrafts in clouds are small and cloud optical thicknesses are thin. Furthermore, the contrast between the CCN concentrations inside ship tracks and the background values are usually quite high. These factors combined produce a more isolated and prominent aerosol indirect effect. Although aerosol indirect effect has been simulated by models ranging from cloud scale to global scale (e.g., Kogan et al., 1995, Lohmann and Feichter, 1997), there are still large uncertainties in quantifying the indirect effect mainly due to the complexities of cloud processes. Observations of aerosol indirect effect of different cloud systems are also uncertain, possibly due to low signal to noise ratio and the difficulty in separating dynamic effects from microphysical effects, which are coupled intimately in all cloud processes.

Deep convection is optically thick and occupy a relatively small area on earth. The first indirect effect of the aerosol (the cloud albedo effect) is generally negligible. The second indirect effect (suppression of the rain formation and extension of the cloud life span) becomes important for this type of clouds. However, the cloud dynamics usually play a dominant role in deep convective clouds. To what extent changing cloud CCN affects the cloud dynamical and radiative properties are still an open question. Recent data analyses (e.g., Rosenfeld, 2000, Andrea, 2004) and model simulations (e.g., Khain et al., 2005) have found some evidences of rain suppression in deep convections. However, opposite aerosol indirect effect (rain enhancement) is also found in various cases, indicating the complexity of the aerosol-cloud-precipitation interactions in deep convection.

Mesosoale Convective Systems (MCSs) are organized synoptic scale deep convection which last for hour, even days. Their frequencies of occurrence are low relative to other precipitation clouds. However, they bring considerable surface rainfall both in tropics and in the summer-time mid-latitudes. For example, Nesbitt et al. (2000) estimates that more than 40% of total surface rainfall in tropical area is from MCSs. Between April to September in the central part of North America, the MCSs contribute 30%~70% of total surface rainfall (Fritsch et al., 1986). In additional to their contributions in hydrological cycle, these MCSs play very important role in driving the atmospheric circulations. How increasing CCN concentration alters the microphysical, dynamical, and radiative properties in these large systems is an important aspect of the global aerosol indirect effect. In this study, we attempt to use a cloud-resolving model (CRM) with a detailed bin spectral microphysical scheme to address this question.

2. MODEL DESCRIPTIONS

The CRM used in this study is the Goddard Cumulus Ensemble (GCE) model (Tao and Simpson, 1993; Tao et al., 2003). Due to the fact that the MCSs usually have quasi 2-D structures, together with the computational burden of the detailed microphysical calculations required in the aerosol-cloud interaction study, the 2-D, anelastic version of GCE model with open lateral boundary conditions is used. The current model includes both solar and infrared radiation, and a bulk aerodynamic surface flux scheme (Tao et al. 1996). The subgrid-scale turbulence in the GCE model is based on Klemp and Wilhelmson (1978). All scalar variables use a forward-in- time, positive-definite advection scheme with a non-oscillatory option (Smolarkiewicz and Grabowski, 1990).

* *Corresponding author address:* Xiaowen Li, Code 613.1, NASA Goddard Space Flight Center, Greenbelt, MD 20771.
E-mail: xli@agnes.gsfc.nasa.gov

The bin microphysical scheme in the Hebrew University Cloud Model (HUCM) has been coupled with the GCE model (e.g., Khain et al, 2005). The HUCM bin microphysical package explicitly describes the size distributions of seven hydrometeor types: cloud/rain, three types of ice crystals (plate, column and branch), snow, graupel, and hail/frozen drops, as well as CCN. The particle size distribution of each hydrometeor type is represented using 33 mass doubling bins, i.e., the mass of the k*th* bin, $m_k=2m_{k-1}$, where $m_1=3.4\times10^{-11}$g (corresponding to the smallest water droplet radius of $r_1=2$ μm). The bin microphysical scheme solves equations of the discrete particle number concentration $f_{i,k}$ ($f_{i,k}dm_k$ is the particle number per unit volume of air whose masses are between m_k and m_k+dm_k), where i=1,7, representing types of different hydrometeors, and k=1,33, representing the sizes of particles. The advections of the term $f_{i,k}dm_k$ use the same scalar advection scheme in the GCE model. The CCN spectrum is also represented by 33 mass size bins with the maximum CCN size the same as the minimum cloud droplet size. Activation of the CCN is explicitly calculated using the Köhler theory without any further assumptions, making this microphysical scheme ideal for studying the CCN-cloud-precipitation interactions. Other microphysical processes simulated in the HUCM include ice nucleation, condensation/ evaporation, deposition/ sublimation, drop-drop, drop-ice, and ice-ice collision and coalescence, collisional breakups of raindrops, ice multiplications, as well as detailed freezing and melting processes.

3. CASE DESCRIPTIONS

Two case studies will be presented here. The characteristics of these two MCSs are summarized in Table 1. The PRE-STORM is a well-organized summer time continental squall line with large CAPE and strong near surface wind shear. In contrast, the TOGA-COARE case represents a typical MCS over the warm ocean, with large precipitable water, relatively less CAPE and less wind shear.

Table 1: Characteristics of MCS cases simulated.

	Location	Time	CAPE (m^2s^{-2})	Precip. Water ($g\,cm^{-2}$)	Richardson Number
PRE-STORM	Oklahoma	Jun 10-11, 1985	2300	4.28	25
TOGA COARE	Tropical Pacific	Feb. 22, 1993	1776	6.33	74

Both case studies use a single sounding in front of the MCS as the homogeneous initial conditions. A single cool pool is applied at the center of the domain in the first 10 minutes to trigger the initial deep convection. The bulk aero-dynamics surface fluxes are applied for the PRE-STORM case, whereas a case specific TOGA surface flux scheme is used for the TOGA COARE case. The horizontal resolution is 1 km for PRESTORM and 0.75 km for TOGA COARE. The horizontal grid points are 1026, with the outer 76 points on each side stretched. There are 33 stretched vertical levels with the highest resolution near the surface. Sponge layers are applied near the upper boundary to absorb the gravity waves.

Due to the lack of the observations of the initial CCN conditions, some idealized CCN spectra are used according to Twomey and Wojciechowski (1969):

$$N_{CCN} = CS^k \qquad (1)$$

where N_{CCN} is the number concentration of the CCN (cm^{-3}), S is the vapor supersaturation respect to water. C and k are constants that change with location, time, height, and air parcel history. In this study, C=600 cm^{-3}, k=0.308 and C=2520 cm^{-3}, k=0.308 are used to represent the clean and dirty scenario of the CCN spectra in the continental PRE-STORM case (Pruppacher and Klett, 1997). The concentrations for CCN particles larger than 0.4 μm are set to be zero in this case. In other word, no giant CCN are present in the PRE-STORM case. Over the ocean, C=100 cm^{-3}, k=0.42 are used to represent the background, clean environment, whereas the dirty continental spectrum with the large CCN tail is used in the dirty scenario. It is assumed that the CCN number concentration does not change with height. Since the emphasis of this study is on the sensitivity of the MCS structure to the initial CCN number concentration, eqn' (1) should provide adequate and straightforward assumption for our purposes. The variations of the shape of the CCN spectra and CCN vertical profiles are important aspects of CCN variability and need to be further studied in the future.

Both PRE-STORM and TOGA COARE cases are long-lasting MCSs with their life spans longer than 12 hours. The model simulations for both cases are carried out for 9 hours, until the model settles well into the quasi-steady state. The average properties of the last 3 hours are taken in the analyses to represent the quasi-steady states of the simulated MCSs.

4. PRE-STORM CASE

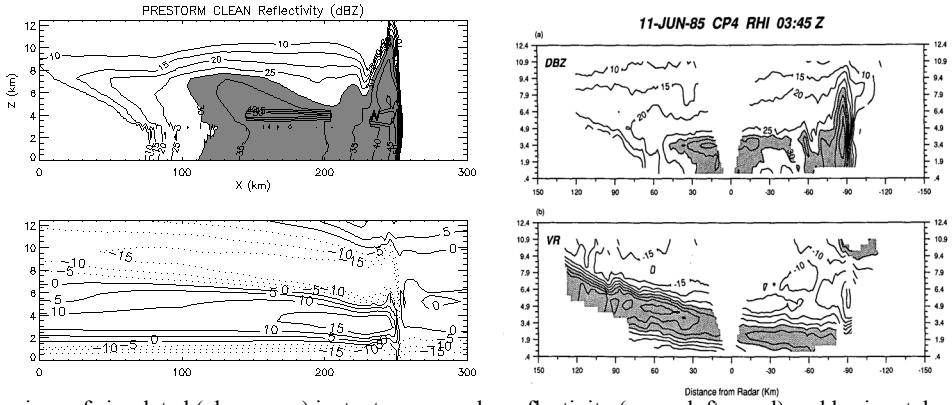

Fig. 1: Comparison of simulated (clean case) instantaneous radar reflectivity (upper left panel) and horizontal wind (lower left panel) with the radar observation (upper right panel) and horizontal wind retrieval (lower right panel). The spatial scale and contour levels are all matched. Areas of radar reflectivity larger than 30 dBZ are shaded grey. The observations are coped from fig. 5 Rutledge et al., 1988.

As a preliminary validation, the simulated instantaneous radar reflectivity and the horizontal air velocity in the clean scenario PRE-STORM case at the end of the simulation are compared with the radar observations during the mature stage of the same storm. All the spatial and contour levels are matched in fig. 1. As shown in the upper panels in fig. 1, the PRE-STORM MCS has a leading convection line on the right hand side, with an extensive trailing stratiform rain to the left. The size of the storm, the maximum radar reflectivity at the leading edge, and the extensive stratiform rain with a prominent bright band all agree well between the simulation and the observation.

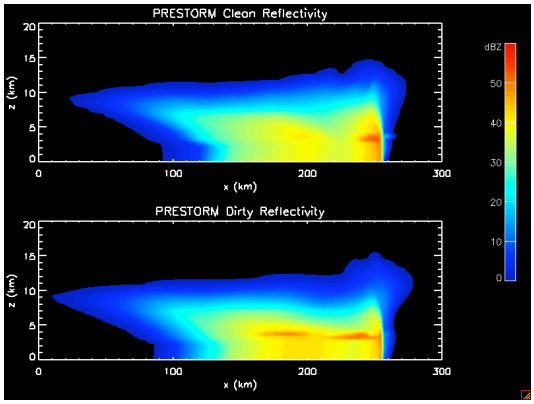

Fig. 2: Simulate radar reflectivity averaged over the last 3 hour's simulations. The upper panel is for the clean scenario, and the lower panel is for the dirty scenario.

The major flow patterns in a MCS are also captured well in the simulation, as shown in the lower two panels in fig. 1. The upper level front to rear outflow, the mid level rear to front inflow, and the near surface outflow beneath the stratiform rain are all simulated with similar strength as in the observation. The biggest discrepancy between the simulation and the observation is the downward bending of the rear to front in flow, which is observed at the lower right panel in fig. 2, but is missing in the simulations at the lower left panel. Lack of large scale forcing, especially mid level vortex to the rear of the system is the reason for the discrepancy. Unfortunately, these large-scale features cannot be simulated properly in the current 2-D frame CRM simulations.

The sensitivity of the PRE-STORM case to different CCN number concentrations is examined by comparing model output in both clean and dirty environment defined in section 3. Figure 2 is the averaged radar reflectivity during the last 3 hours' simulation, representing the quasi-steady state MCS structure under clean and dirty environment, respectively. From fig. 2 we see that the general structure of the PRE-STORM case in both clean and dirty environment are very similar, with a leading convection and extended trailing stratiform region. The dirty scenario produces slightly wider stratiform rain. During the last 3 hours' simulation, clean case has a domain average of 44.2 mm/day surface rainfall, among which ~51% comes from the stratiform rain. On the other hand, the surface rainfall is 38.3 mm/day for the same period for the dirty case, with ~73% contributed by the stratiform rain.

Figure 3 is the time series of the domain averaged surface rainfall rate for the clean and dirty scenario simulations. The delay of the onset of surface rainfall in the dirty case is clearly caused by the reduction of the cloud droplet sizes, thus increase the time needed for rain formation. In terms of the total surface rain, increasing CCN concentration in the PRE-STORM case has an overall effect of reducing the total surface rainfall. Unlike the shallow convection cases where warm rain is dominant, the ice microphysical processes play a crucial role in reducing and redistributing the surface rainfall. In the deep leading convection, increasing CCN number concentration produces more numerous, but smaller cloud droplets. It is harder to form large raindrops with smaller cloud droplets. Therefore, more cloud water is

transported to above the freezing level, producing more super –cooled water at upper levels in the dirty scenario simulation. Furthermore, these smaller cloud droplets are harder to be collected by the large, fast falling graupel or hail particles. Compared with the clean scenario simulation, more cloud water is transformed into the slow falling ice particles (snow and ice crystals) through freezing or depositional growth in the dirty scenario simulation. These slow falling ice particles are transported by the upper level front to rear outflow to the stratiform region, generating more extensive and intense stratiform rain there. The dashed lines in fig. 3 represent the total stratiform rain simulated in the PRE-STORM case. It is found that the stratiform portion of the total surface rain increases much faster with time in the dirty scenario simulations, indicating the enhanced rearward transport of the hydrometeors.

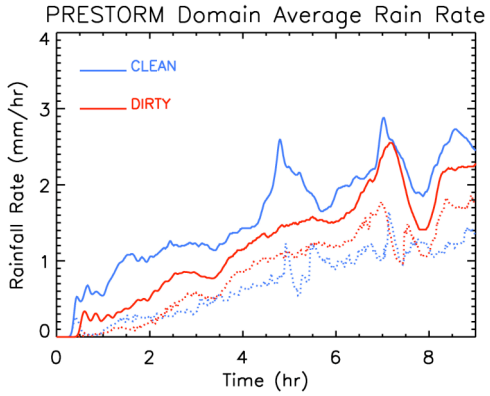

Fig. 3: Domain averaged time series of the surface rainfall rate (mm/hr) for the clean (blue line) and dirty (red line) cases. The dashed lines represent the contribution of the stratiform rain to the total surface rainfall.

4. TOGA COARE CASE

Airborne radar observation of Feb. 22, 1993 TOGA COARE MCS is plotted in figure 4, together with the instantaneous simulated radar reflectivity at t=340 min for the clean scenario. Again, the spatial scale and contour levels are matched for both the simulation and the observation. Similar storm size, structure and surface radar reflectivity pattern are found in both the observation and the simulation, indicating the capability of the GCE model in simulating MCSs in vastly different environmental conditions. Both the PRE-STORM and TOGA COARE comparisons show higher simulated radar reflectivity above the melting level in the stratiform region. This may be caused by the simplification in our theoretical calculations of the radar reflectivity of ice phase particles. Likewise, the simulated radar bright bands in both cases are more prominent than the observations, which is associated with the uncertainties in calculating radar backscattering cross section of melting particles.

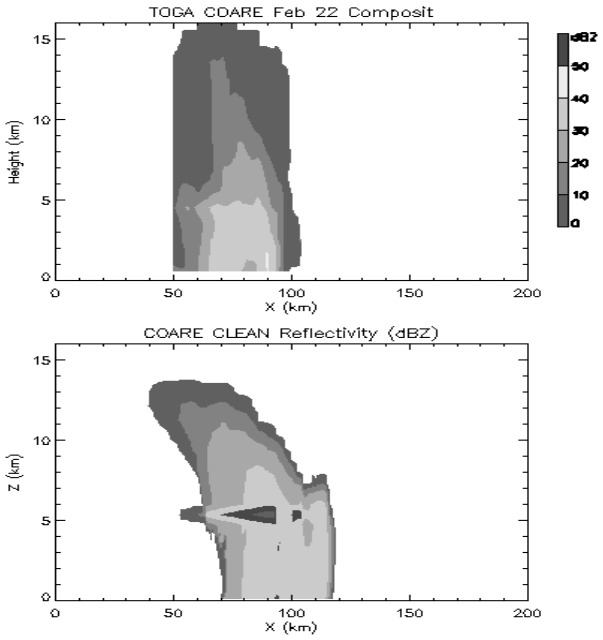

Fig. 4: Comparison of the observed radar reflectivity (upper panel) and simulated instantaneous radar reflectivity (lower panel) for the TOGA COARE case MCS. The radar observation data are provided by Jorgensen at NOAA.

Compared with the PRE-STORM case, TOGA COARE MCS has a much smaller stratiform region and is less organized. Model simulations show that these differences are mainly the results of the different thermodynamic conditions in these two difference cases. Even before taking into account the differences of the CCN concentrations (e.g., in bulk microphysical scheme simulations), the TOGA COARE case has weaker updrafts and smaller amount of ice and super cooled water aloft.

To the contrary of the rain suppression effect in the dirty environment as simulated in the PRE-STORM case, increasing CCN concentration in the TOGA COARE case *enhances* surface rainfall and storm intensity. Figure 5 is the averaged radar reflectivity during the last 3 hours' simulation in TOGA COARE case for the clean and dirty scenario simulations. Unlike the PRE-STORM case in fig. 2, changing initial CCN in this maritime MCS changes both the storm structure and intensity. In the lower panel of fig. 5, the leading convection is obviously stronger in the dirty scenario simulation, with the 30 dBZ level near 10 km height. On the other hand, the clean scenario simulations has the 30 dBZ level at around 7 km, less than 2 km above the melting level. The vertical velocity plots (not shown) confirms the increase of the updraft intensity at the leading convection when CCN concentration is increased. In the clean environment, the vast majority of the surface rainfall comes from warm rain process, whereas ice

microphysics play a much more significant role in the dirty scenario simulation. This is also the reason of a more extensive stratiform area and stronger stratiform rain intensity in the dirty scenario simulation, as shown in fig. 5.

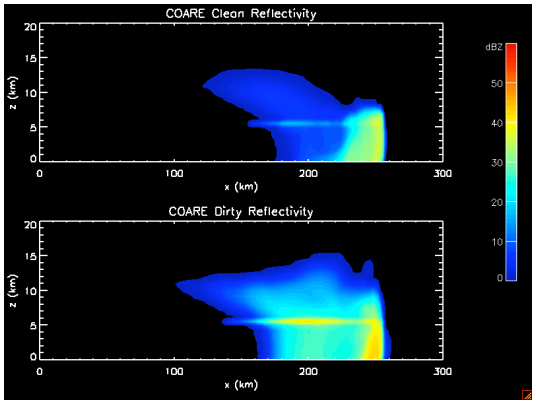

Fig. 5: The same as fig. 2, except for the TOGA COARE case.

Similar to fig. 3, the domain averaged time series of surface rainfall are plotted in fig. 6. Consistent with the PRE-STORM case simulations, increasing CCN number concentration delays the onset of the surface rainfall in the TOGA COARE case, too. This further supports the classical aerosol indirect effect proposed by Twomey. However, the suppression of surface rainfall happens only in the first half an hour's simulation. After that, the surface rainfall rate for the dirty scenario quickly intensifies and surpasses the average surface rain in the clean scenario. At around t=4 hours, the rainfall rate in the clean simulation increases to a maximum, too, which is comparable to the value of the surface rainfall in the dirty case. However, after 4 hours, the regenerating convection in the clean case remains mainly warm rain, with the cloud top mostly below 7 km, and very little trailing stratiform rain. On the other hand, the dirty scenario simulation maintains a strong leading convection which transports significant amount of ice particles rearward into the stratiform region, keeping the typical leading convection/trailing stratiform MCS prototype, as well as higher surface rainfall rate.

5. SUMMARY AND FUTURE WORK

Aerosol indirect effect to the long-lasting, deep MCS systems are investigated by using a CRM with a detailed spectra bin cloud microphysical and CCN activation scheme. Two MCS systems formed under very different environments are studied here: one is a strong, well-organized continental squall line (PRE-STORM), the other is a less organized, smaller MCS over tropical western Pacific (TOGA COARE).

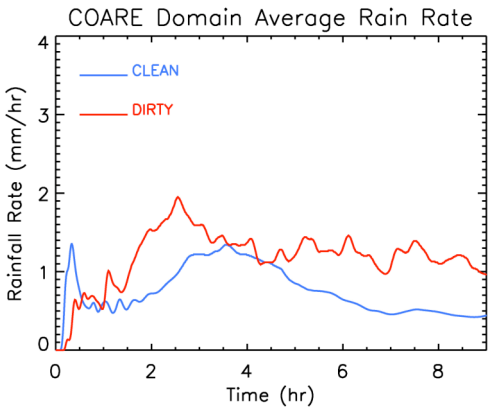

Fig. 6: The same as fig. 3, except for the TOGA COARE case simulations.

The long-term model simulations using typical CCN spectra of the continental and oceanic environment as clean scenarios, and a polluted continental CCN spectrum as the dirty scenario are carried out using 2-D GCE model. The simulations show opposite aerosol indirect effects in two different cases. In the PRE-STORM case, increasing CCN concentration suppresses the total surface rainfall but enhances the stratiform rain portion of the squall line. Increasing CCN concentration does not alter the storm dynamics and structure significantly. The reduced cloud droplet sizes caused by the aerosol indirect effect result in more slow-falling ice particles at the upper levels of the leading convection. These ice particles are subsequently transported to the rear of the squall system and enhance the stratiform rain.

Increasing CCN concentration in the TOGA COARE case only delays/suppresses the surface rainfall at the initial stage of the system development. However, during the quasi-steady state of the simulated MCS, increasing CCN concentration actually enhances the storm intensity. Further sensitivity tests and diagnostic studies are currently underway to determine the robustness of this "anti-aerosol indirect effect" and to unravel the mechanisms behind this effect.

The two case studies of the aerosol indirect effect on the long-lasting MCSs show opposite signs. This indicates the complexity of the cloud microphysics/dynamics interactions and their interactions with the large-scale environment. Simple extrapolations of the classical aerosol indirect effect to other highly nonlinear cloud systems are certainly not sufficient in studying the global average aerosol indirect effect.

Reference:

Andrea, M. O., D. Rosenfeld, P. Artaxo, A. A. Costa, G. P. Frank, K.-M. Longo, and M. A. F. Silva-Dias, 2004: Smoking rain clouds over the Amazon. *Science*, **303,** 1337-1342.

Coakley, J. A., Jr., R. L. Bernstein, and P. A. Durkee, 1987: Effect of ship-stack effluents on cloud reflectivity. *Science,* **237,** 1020-1022.

Ferek, R. J., T. Garrett, P. V. Hobbs, S. Strader, D. Johnson, J. P. Taylor, K. Nielsen, A. S. Ackerman, Y. Kogan, Q. Liu, B. A. Albrecht, and D. Babb, 2000: Drizzle suppression in ship tracks. *J. Atmos. Sci.,* **57**, 2707-2728.

Fritsch, J. M., R. J. Kane, and C. R. Chelius, 1986: The contribution of mesoscale convective weather systems to the warm-season precipitation in the United State. *J. Climate and Appl. Meteor.,* **25,** 1333-1345.

Khain, A., D. Rosenfeld, and A. Pokrovsky, 2005: Aerosol impact on the dynamics and microphysics of deep convective clouds. *Q. J. R. Meteor. Soc.,* **131,** 2639-2663.

Klemp, J. B., and R. B. Wilhelmson, 1978: The simulation of three-dimensional convective storm dynamics. *J. Atmos. Sci.,* **35,** 1070-1096.

Kogan, Y. L., M. P. Khairoutdinov, D. K. Lilly, Z. N. Kogan, and Q. Liu, 1995: Modeling of stratocumulus cloud layers in a large eddy simulation model with explicit microphysics. *J. Atmos. Sci.*, **52,** 2923-2940.

Lohmann, U., J. Feichter, Impact of sulfate aerosols on albedo and lifetime of clouds: A sensitivity study with the ECHAM4 GCM, J. Geophys. Res.,102(D12),13685-13700,10.1029/ 97JD00631, 1997.

Nesbitt, S. W, E. J. Zipser, and D. J. Cecil, 2000: A census of precipitation features in the tropics using TRMM: Radar, ice scattering, and lightning observations. *J. of Climate,* **13**, 4087-4106.

Rosendeld, D., 2000: Suppression of rain and snow by urban and industrial air pollution. *Science,* **287**, 1793-1796.

Rutledge, S. A., R. A. Houze, Jr., and M. I. Biggerstaff, 1988: The Olkahoma-Kansas mesoscale convective system of 10-11 June 1985: Precipitation structure and single-doppler radar analysis. *Mon. Wea. Rev.,* **116**, 1409-1430.

Smolarkiewicz, P. K., and W. W. Grabowski, 1990: The multidimensional positive advection transport algorithm: nonoscillatory option. *J. Comput. Phys.,* **86,** 355-375.

Tao, W.-K. and J. Simpson, 1993: Goddard Cumulus Ensemble Model. Part I: Model description. *Terr. Atmos. Oceanic Sci.,* **4,** 35-72.

_____, S. Lang, J. Simpson, C.-H. Sui, B. Ferrier, and M.-D. Chou, 1996: Mechanisms of cloud-radiation interaction in the tropics and midlatitudes. *J. Atmos. Sci.,* **53,** 2624-2651.

_____, J. Simpson, D. Baker, S. Braun, M.-D. Chou, B. Ferrier, D. Johnson, A. Khain, S. Lang, B. Lynn, C.-L. Shie, D. Starr, C.-H. Sui, Y. Wang, and P. Wetzel, 2003: Microphysics, radiation and surface processes in the Goddard Cumulus Ensemble (GCE) model. *Meteorol. Atmos. Phys.,* **82,** 97-137.

Twomey, S., 1977: The influence of pollution on the shortwave albedo of clouds. *J. Atmos. Sci.*, **34,** 1149-1152.

Twomey, S. A., M. Piepgrass, and T. L. Wolfe, An assessment of the impact of pollution on global cloud albedo, *Tellus, 36B*, 356-366, 1984.